Control of near-field polarizations for nanoscale molecular orientational imaging

T. Mino,[1] Y. Saito,[1,2,a)] and P. Verma[1]
[1]Department of Applied Physics, Osaka University, 2-1 Yamadaoka, Suita, Osaka 565-0871, Japan
[2]Department of Chemistry, Gakushuin University, 1-5-1 Mejiro, Toshima, Tokyo 171-0031, Japan

(Received 3 June 2016; accepted 18 July 2016; published online 28 July 2016)

Polarization-controlled tip-enhanced near-field Raman spectroscopic imaging is demonstrated using two characteristic dipoles induced at a metallic nano-tip. The polarization generated at the tip can be considered as a single dipole that can be switched from *s* to *p* by modulating the incident laser polarization. The *s*-dipole achieves highly selective molecular orientation imaging, while *p*-polarization provides comprehensive imaging in all directions. We discuss the controllability of near-field polarizations through the evaluation of the dipole orientation induced at the nano-tip. Polarization control and switching in near-field imaging are of tremendous advantage, as they allow the study of the molecular orientations in a sample, along with spectroscopic information. *Published by AIP Publishing*. [http://dx.doi.org/10.1063/1.4960016]

Molecular orientations and assemblages often play an essential role in determining the function of a material, such as electron transport, filtering, and optical memories.[1–3] Therefore, a spectroscopic imaging technique based on polarization-controlled illumination can be a valuable tool for studying the unique properties of a sample. Polarization treatment under extremely high spatial resolution, particularly in nano-spectroscopy, requires special attention.[4,5] In aperture-less near-field spectroscopy, the depolarization effect caused by a metallic nano-tip results in unique polarization properties, which are different from the conventional microscopy. Tip-enhanced Raman spectroscopy (TERS), one of the well-used techniques among near-field microscopies, utilizes a metallic nano-tip that is brought near the sample at the focal spot of the illumination that detects the vibrational spectra of a molecule and directly reflects the chemical composition of a sample.[6–8] Owing to the resonant excitation of the localized surface plasmon polaritons (LSPPs), a strongly enhanced and highly confined light field is created in close proximity to the tip apex, which provides super-high spatial resolution in TERS measurements.[9] So far, TERS has been applied to resolve local variations in the Raman spectra that would be hidden in far-field measurements.[10–14] Analysis of molecular orientation is an important issue for TERS as well as for conventional Raman spectroscopy, especially in the field of material science, to control the physical and chemical properties of molecular films.[15–19] The near-field polarization was also studied by photo induced structure of azo-polymers irradiated with a metallic nano-tip.[18,19] It is generally believed that the incident polarization is not preserved in the near-field at the tip apex, but rather a new distribution of light polarization is created. We have recently developed a method to analyze the polarization of near-field light in TERS from the scattering pattern produced by the nano-tip.[20] The induced field pattern at the apex of the nano-tip can be approximated as a single dipole, because only the silver nano-particle at the tip apex, which is much smaller than the wavelength of the incident laser, contributes to the near-field imaging under an evanescent illumination. In the previous report, we experimentally confirmed that the direction of the dipole oscillation at the apex of the tip determines the polarization of near-field light. By employing several metallic tips having different dipoles, we performed polarization-TERS imaging of single-walled carbon nanotubes (SWNTs) with contrast reflecting the geometry of the tubes. Quantitative near-field polarization analysis has thus become possible. The next step is the control and switching of the induced dipoles.

In this study, we demonstrate orientation-selective TERS imaging employing two characteristic dipoles induced at a metallic nano-tip. The dipoles were switched by setting the incident polarization to either *s* (parallel to the sample plane) or *p* (perpendicular to the sample plane). The nano-imaging of SWNTs was performed by employing these dipoles.

The TERS system is based on a transmission-mode atomic force microscopy (AFM)-controlled setup described elsewhere.[12–14] The excitation laser wavelength was 488 nm continuous wave (CW), and the laser was focused on the sample plane by a $\times 60$ objective lens having NA = 1.4. TERS measurements were performed using an *s* or *p* polarization. We generated radially polarized light for a *p*-polarized excitation by using an eight-segmented half-wave plate (Z-pol, Nanophoton Inc., Japan)[21] and a linear polarizer oriented along the *x* direction for *s*-polarized excitation. Raman scattering light was directed to the spectrometer, which was then detected by a liquid-nitrogen-cooled CCD camera. The TERS measurements were performed in a 1280×640 nm area with a step of 20 nm. The power of the incident laser light at the sample was 150 μW, and the exposure time at each point was 0.4 s. The tips, each of which featured a 60-nm-thicksilver-coating, were prepared by thermal evaporating on commercially available silicon cantilevers used in contact-mode AFM.[22] In order to prepare our SWNT samples, we dissolved the commercially purchased SWNTs in 1,2-dichloroethane by ultrasonication. The supernatant was poured on a cover glass heated by a hot plate to fix the sample onto the substrate. The polarization of the near-field light confined at the apex of a

a)yuika.saito@gakushuin.ac.jp

given metal-coated TERS tip was determined precisely by defocus imaging; the details of this procedure have been reported elsewhere.[20] The intensity distribution within a laser focus spot was measured by detecting the Rayleigh scattering light using a photo detector while scanning the tip near the focus.

The field component at the apex of the metallic tip was calculated within the framework of the coupled dipole formalism by using Green's function.[23–25] The metal-coated tip was modeled as a cone with a cone angle of 14°, placed 5 nm above a glass substrate. The apex was approximated as a 60-nm-diametersphere made of pure silver. The illumination configuration was the same as the actual experimental setup: 488-nm excitation wavelength by evanescent illumination ($1 < \mathrm{NA} < 1.4$). The calculation was performed on an xy-plane 3 nm away from the tip apex, with the calculation step set to 0.75 nm.

Supposing the apex of a metallic tip is a perfect sphere placed in a vacuum, the induced tip dipole would be exactly the same as an incident laser polarization. In actual experimentation, owing to the random shape and size of the evaporated silver nanoparticles, particularly those at the apex of the tip, such perfect controllability cannot be realized, even when the tips are fabricated under identical conditions. However, the average properties can still be manipulated by the electric field of the incident laser. Figure 1(a) is the scanning electron microscopy (SEM) image of the metallic nano-tip used in our experiments. The apex of the tip consists of many silver particles attached randomly on an oxide silicon probe. It is not possible to estimate the polarization properties of the tip from the SEM images alone, which suggests that the polarization properties and the metal structures are not directly linked although the single particle at the apex is the main contributing factor to the tip dipole. Figs. 1(b) and 1(c) illustrate the orientation of the induced dipole experimentally obtained under x- and z-polarization excitations. The orientation of the dipole can be characterized by two parameters, namely, the tilt angle from the z-axis (θ) and the in-plane rotation angle from the x-axis (ϕ). The dipole directions determined from the defocus image (shown in insets) are $\theta = 65°$ and$\phi = 15°$ for x-polarization and $\theta = 15°$ and $\phi = 85°$ for z-polarization excitations. In Fig. 1(b), the small ϕ and relatively large θ indicate that the induced dipole is approximately in the direction of the x-axis, reflecting the direction of the incident polarization. In Fig. 1(c), on the other hand, the small θ indicate that the dipole is in the z-direction, also influenced by the incident laser polarization. For convenience, the former will be referred to as "x-dipole" and the latter as "z-dipole." The results in Fig. 1 show that the tip dipole is not perfectly controlled but strongly influenced by the incident polarization. The switching of the tip dipole is of practical importance because polarization imaging usually requires information obtained from two orthogonal directions, but even more importantly, because it is not desirable to replace the tip during TERS measurements. In the experimental configuration of transmission-mode TERS, the formation of a p-dipole is favored over an s-dipole, owing to the shape of the metallic tip. As indicated in Fig. 1(b), even though x-polarization excitation was employed, θ is still 65°.

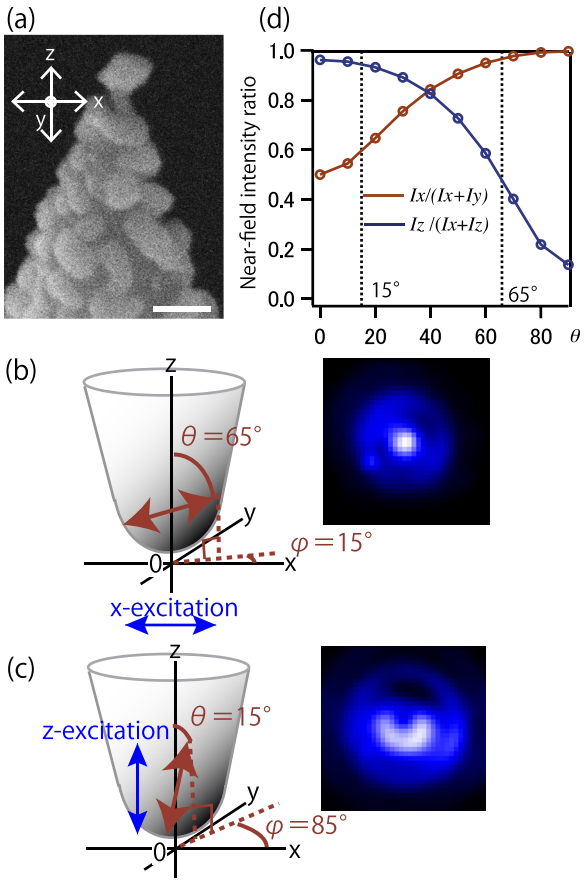

FIG. 1. Characterization of the tip dipole. (a) SEM image of a silver-coated tip, the scale bar indicate 100 nm, (b) the defocus images of the induced tip dipoles excited by linearly, and (c) radially polarized incident light. The angles of the induced dipoles were determined by the least-squares fitting of the defocused images as $\theta = 65°\phi = 15°$ for (b) and $\theta = 15°\phi = 85°$ for (c). (d) Calculated polarization selectivity in the x-y and x-z directions with respect to the angle θ. The red line represents the ratio $Ix/(Ix + Iy)$ and the blue line represents $Iz/(Ix + Iz)$. The θ obtained in our experiments are indicated by the dotted lines.

The polarization selectivity in the x, y, or z directions is strongly dependent on the dipole angle θ. For further discussion, the near-field intensities Ix, Iy, and Iz, generated by the tip dipole were defined. The red line in Fig. 1(d) plots the calculated polarization component ratio $Ix/(Ix + Iy)$ as a function of θ. This ratio achieves a value of 0.5 when Ix and Iy are equal, indicating no sensitivity of polarization, whereas it achieves a value of 0 or 1 when Ix or Iy is zero, respectively, indicating a perfect polarization selectivity in the y or x direction for these values. The values of θ determined in our experiment are also shown as the dotted lines. By employing a p-dipole (small θ), the polarization selectivity is relaxed as the polarization component ratio is near 0.5, while by employing an s-dipole (large θ), a strong selectivity in the in-plane (x,y) direction is achieved as the ratio reaches near 1. The blue line in Fig. 1(d) plots the calculated $Iz/(Ix + Iz)$ ratio versus θ. It can easily be expected that Iz will decrease with increasing θ; however, a significant intensity remains even at $\theta = 90°$. These results suggest that perfect polarization selectivity in all three orthogonal directions is impossible in near-field experiments, owing to the dipole properties of the metallic tip, although partial manipulation is still of great importance for quantitative TERS analysis.

Figures 2(a) and 2(b) show TERS images taken by the *x*- and *z*-dipoles, respectively. The sample contained some bundled SWNTs in various orientations, and the image contrast was constructed from the intensity of the G^+-band. An AFM topographic image taken from the same sample area is shown in Fig. 2(c). As estimated from the height in the AFM image, each bundle contained a few tens of SWNTs. The Raman vibration of SWNTs under resonant conditions is known to be parallel to the long axis of the SWNT; thus, the contrast of a G^+-band intensity image can be predicted from the polarization state and the molecular orientation, which can easily be determined from a topographic image.[26] The excitation polarization parallel to the nanotube axis is the most advantageous to the G^+-band intensity due to the direction of the Raman transition moment. Fig. 2(a) indicates that the tubes aligned in the *x* direction were clearly imaged, while the tubes aligned in the *y* direction were barely imaged. This is clearly due to the *x*-dipole, which creates strong electric field oscillations; selectivity enhances the *x*-Raman vibrations in the sample. On the other hand, the tubes aligned in the *x* and *y* directions were both clearly imaged in Fig. 2(b). This indicates that the *z*-dipole is effective for comprehensive near-field imaging in the *xy* plane where the polarization selectivity was relaxed. More importantly, it shows that significant *s*-polarization components can be obtained from the *z*-dipole, owing to the depolarization effect of the metallic tip. According to the AFM image in Fig. 2(c), the average tube heights in the *x* and *y* directions were 1.37 nm and 3.14 nm, respectively. The average Raman intensities, as determined from Fig. 2(b), were 299 cnt and 801 cnt for the tubes in *x* and *y* alignments, respectively. Thus, the TERS signal counts were estimated to be 218 cnt/nm and 255 cnt/nm for the *x* and *y* directions, respectively.

The near-field image contrast can be attributed to the electric field components generated under the tip dipole. Figure 3 shows the calculated *x*, *y*, and *z* field intensity distributions under the metallic tip. Figs. 3(a)–3(c) show the *x*, *y*, and *z* polarization components induced by the *x*-dipole, and Figs. 3(d)–3(f) show the *x*, *y*, and *z* polarization components induced by the *z*-dipole. A comparison of Figs. 3(a) and 3(b) reveals that the intensity of the *x*-polarization component is an order of magnitude larger than that of the *y* component. Thus, it is confirmed that the *x*-dipole is responsible for the image selectivity in the *x*-direction. Unlike the *x*-dipole, the intensities of the *x* and *y* field components were comparable in Figs. 2(d) and 2(e), pointing to moderate polarization selectivity with the *z*-dipole. In fact, the ratio of the average intensities of (d)–(e) was 1:1.2, which is quantitatively consistent with the experimentally obtained signal intensity, discussed in the above paragraph. When the dipole becomes highly *z*-oriented, the field distributions in the *xy* plane appear to be identical as seen in Figs. 3(c) and 3(f). The dipole analysis in Fig. 1(c) suggests that the induced dipole is highly *z*-polarized ($\theta = 15°$), which means that the value of ϕ plays a less important role than in contrast formation.

The spatial distribution properties of the intensity are responsible for the formation of near-field images. In Fig. 2(b), a tube aligned in the *x* direction was appeared slightly winded in the near-field image. We presume that this deformation is a consequence of the field pattern in Fig. 3(d), showing two identical intensity maxima.

We note that a strong *z*-polarization field co-exists in TERS measurements, which are important for the observation

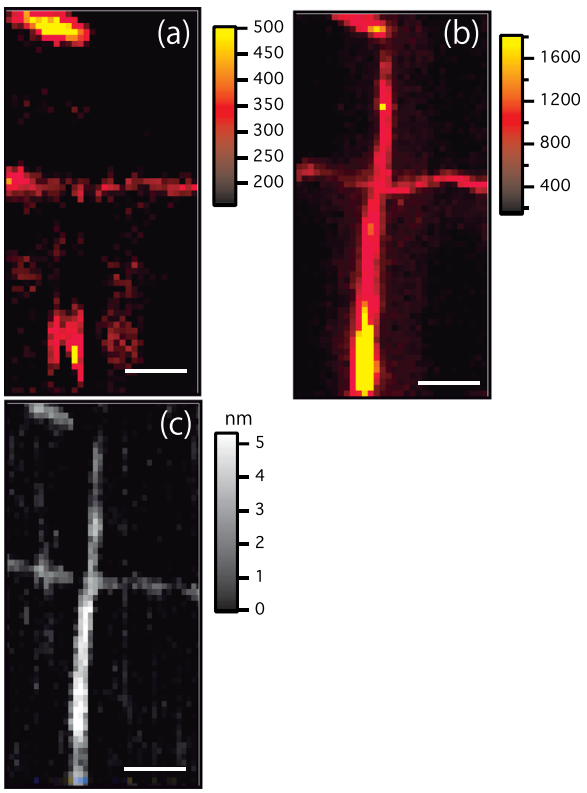

FIG. 2. TERS images of SWNTs (a) measured by the *x*-dipole and (b) the *z*-dipole. (c) AFM image of the corresponding area. The scale bars represent 200 nm.

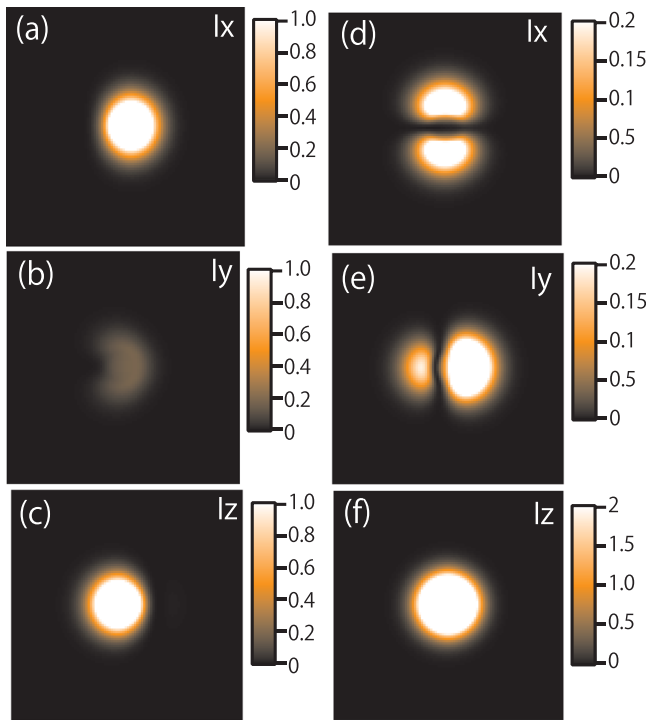

FIG. 3. Calculated near-field intensity and the spatial distribution of the polarization components *Ix*, *Iy*, and *Iz*, generated by the *x*-dipole ((a), (b), and (c), respectively) and by the *z*-dipole ((d), (e), and (f), respectively) defined in Figs. 1(b) and 1(c). The calculation area was 75 nm^2.

of Raman transitions in the z-direction and also of off-diagonal Raman tensor components, although the detection efficiency of a z-dipole is small compared to that of an x- or y-dipole. Since the strongest Raman transition moment is parallel to the long axis of the tube in SWNTs, the z-dipole does not contribute to the Raman signal when the tube lies on the substrate. In contrast, a pentacene molecule for example, which is often used to produce organic transistors, should ideally attach perpendicularly to the substrate to form a thin film.[27,28] In that case, the z-dipole plays a critical role in the analysis of the variation in molecular tilt, which greatly affects the carrier mobility of the transistor.[29]

Besides incident polarizations, another crucial factor which must be taken into account is then on-uniformity of the laser focus. It has been known that the polarization distribution within an incident laser focus is not uniform. By employing a linear polarization as the excitation, we find double intensity peaks for the z-polarization component and a single peak at the center for the x-polarization component. On the other hand under radial polarization, we find a single peak at the center for the z-polarization component, while the other components appear at the circumference.[30] This clearly affects the induced dipole, depending on the tip position within the focus. We experimentally checked the variation of the tip-dipole for tip positioning within the focus. Figure 4(a) shows the experimentally measured intensity distribution of the laser focus using an incident light with radial polarization. The tip apex was placed at three different positions, which were 100 nm apart from each other, as indicated by the crosses. The defocus images obtained at each position are shown in Fig. 4(b). The variations in ϕ and θ obtained from the images are also shown in the figures. When the tip was at the center of the focus (position 2), the dipole was highly z-oriented ($\theta = 30°$) owing to the radial polarization, while at the circumference (positions 1 and 3), this condition was relaxed. Fig. 4(b) experimentally verifies the excitation

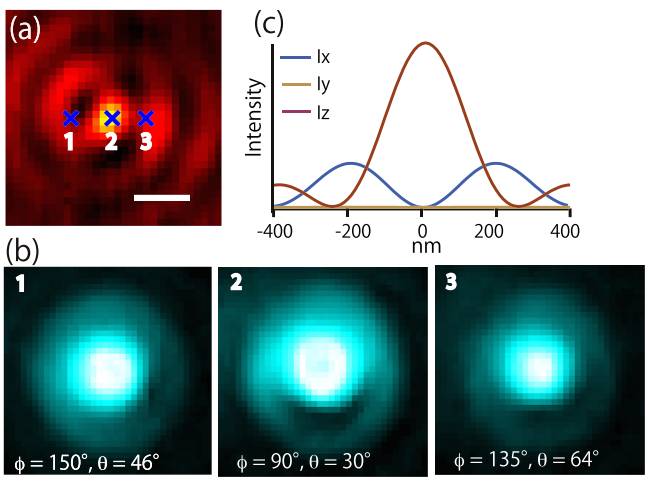

FIG. 4. The effect of tip positioning within a laser focus having polarization inhomogeneity. (a) Intensity distribution of the incident laser by radial polarization incidence. The crosses indicate three positions, which are 100 nm apart from each other, to check the dipole orientations. The scale bar represents 200 nm. (b) Defocused images obtained by placing the nano-tip obtained at positions 1, 2, and 3. The dipole orientations (ϕ, θ) obtained from the defocused images are presented. (c) Calculated polarization component distribution of the z-polarized incident laser focused by 1.4 NA objective lens. The profile shows the cross section of the xz-plane.

inhomogeneity caused by the tightly focused laser spot. The calculated intensity of each polarization component is illustrated in Fig. 4(c). When the tip was placed at the center of the focus, the incident field was highly z-polarized and the x-polarized incident field gradually appeared as the tip moved away. In our experiment, the metallic tip was placed at the center of the focus within an accuracy of ± 20 nm. This is accurate enough compared to the polarization inhomogeneity within the laser focus, which is on the order of 100 nm. Thus, our experiments yield accurate information about the trends characterizing the incident polarizations.

In this work, the polarization controllability of TERS was discussed on the basis of the dipole orientation induced at the nano-tip. We confirmed that even when the metallic nanoparticle attached to the tip apex was of a random shape, the induced dipoles reasonably followed the direction of the incident polarization when the tip was placed at the center of the focus. This property enabled us to perform polarization-selective nano-imaging and allow to switch the near-field polarization during TERS experiments without changing the tip. Using a SWNT sample, a good orientational selectivity in the x-direction was obtained under linear polarization excitation. This would be useful for directional imaging of polymer domains and semiconductor crystal facets for device development.[31–33] On the other hand, the in-plane selectivity was relaxed under radial polarization incidence. This would be useful for comprehensive material mapping of unidentified samples as well as the z-polarized samples. The image contrasts were explained by the induced dipoles on the metallic tip, with the aid of theoretical simulations. It was confirmed that the z-dipole can also be used for xy imaging because the depolarization component of a metallic tip is high enough to provide the in-plane signals.

When optical microscopy is combined with polarization-controlled illumination, it is possible to reveal the distinct characteristics of a sample. We hope that our polarization analysis will help to elucidate the source of the contrast in near-field images, enabling an accurate nanoscale analysis using a TERS microscope.

The authors would like to acknowledge the financial support from Grant-in-Aid for Scientific Research (C) 24560028 and JSPS Core-to-Core Program.

[1]G. S. Harms, M. Sonnleitner, G. J. Schutz, H. J. Gruber, and T. Schmidt, "Single-molecule anisotropy imaging," Biophys. J. **77**, 2864–2870 (1999).
[2]C. Sourisseau, "Polarization measurements in macro- and micro-Raman spectroscopies molecular orientations in thin films and AZO-dye containing polymer systems," Chem. Rev. **104**, 3851–3891 (2004).
[3]D. R. T. Zahn, G. N. Gavrila, and G. Salvan, "Electronic and vibrational spectroscopies applied to organic/inorganic interfaces," Chem. Rev. **107**, 1161–1232 (2007).
[4]Y. Saito and P. Verma, "Polarization controlled Raman microscopy and nanoscopy," J. Phys. Chem. Lett. **3**, 1295–1300 (2012).
[5]S. S. Kharintsev, A. I. Fishman, S. G. Kazarian, and M. K. Salakhov, "Polarization of Near-field light induced with plasmonic nanoantenna," Phys. Rev. B **92**, 115113 (2015).
[6]N. Hayazawa, Y. Inouye, Z. Sekkat, and S. Kawata, "Near-field Raman imaging of organic molecules by an apertureless metallic probe scanning optical microscope," J. Chem. Phys. **117**, 1296–1301 (2002).
[7]R. M. Stockle, Y. D. Suh, V. Deckert, and R. Zenobi, "Nanoscale chemical analysis by tip-enhanced Raman spectroscopy," Chem. Phys. Lett. **318**, 131–136 (2000).

[8]A. Hartschuh, E. J. Sanchez, X. S. Xie, and L. Novotny, "High-resolution near-field Raman microscopy of single-walled carbon nanotubes," Phys. Rev. Lett. **90**, 095503 (2003).
[9]Y. Inouye and S. Kawata, "Near-field scanning optical microscope with a metallic probe tip," Opt. Lett. **19**, 159–161 (1994).
[10]Y. Saito, M. Motohashi, N. Hayazawa, M. Iyoki, and S. Kawata, "Nanoscale characterization of strained silicon by tip-enhanced Raman spectroscope in reflection mode," Appl. Phys. Lett. **88**, 143109 (2006).
[11]D. Zhang, U. Heinemeyer, C. Stanciu, M. Sackrow, K. Braun, L. E. Hennemann, X. Wang, R. Sholz, F. Schreiber, and A. J. Meixner, "Nanoscale spectroscopic imaging of organic semiconductors films by plasmon-polariton coupling," Phys. Rev. Lett. **104**, 056601 (2010).
[12]T. Yano, T. Ichimura, S. Kuwahara, F. H'Dhili, K. Uetsuki, Y. Okuno, P. Verma, and S. Kawata, "Tip-enhanced nano-Raman analytical imaging of locally-induced strain distribution in carbon nanotubes," Nat. Commun. **4**, 2592 (2013).
[13]J. Yu, Y. Saito, T. Ichimura, S. Kawata, and P. Verma, "Far-field free tapping-mode tip-enhanced Raman microscopy," Appl. Phys. Lett. **102**, 123110 (2013).
[14]Y. Okuno, Y. Saito, S. Kawata, and P. Verma, "Tip-enhanced Raman investigation of extremely localized semiconductor-to-metal transition of a carbon nanotube," Phys. Rev. Lett. **111**, 216101 (2013).
[15]M. Tanaka and R. J. Young, "Polarised Raman spectroscopy for the study of molecular orientation distributions in polymers," J. Mater. Sci. **41**, 963–991 (2006).
[16]R. V. Maximiano, R. Beams, L. Novotny, A. Jorio, and L. G. Cançado, "Mechanism of near-field Raman enhancement in two-dimensional systems," Phys. Rev. B **85**, 235434 (2012).
[17]X. Wang, K. Broch, F. Schreiber, A. J. Meixner, and D. Zhang, "Revealing nanoscale optical properties and morphology in perfluoropentacene films by confocal and tip-enhanced near-field optical microscopy and spectroscopy," Phys. Chem. Chem. Phys. **18**, 15919 (2016).
[18]H. Ishitobi, M. Tanabe, Z. Sekkat, and S. Kawata, "Nanomovement of azo polymers induced by metal tip enhanced near-field irradiation," Appl. Phys. Lett. **91**, 091911 (2007).
[19]G. D. Florio, E. Bründermann, N. S. Yadavalli, S. Santer, and M. Havenith, "Polarized 3D Raman and nanoscale near-field optical microscopy of optically inscribed surface relief gratings chromophore orientation in azo-doped polymer films," Soft Matter **10**, 1544–1554 (2014).
[20]T. Mino, Y. Saito, and P. Verma, "Quantitative analysis of polarization-controlled tip-enhanced Raman imaging through the evaluation of the tip dipole," ACS Nano **8**, 10187–10195 (2014).
[21]Y. Saito, N. Hayazawa, H. Kataura, T. Murakami, K. Tsukagoshi, Y. Inouye, and S. Kawata, "Polarization measurements in tip-enhanced Raman spectroscopy applied to single-walled carbon nanotubes," Chem. Phys. Lett. **410**, 136–141 (2005).
[22]N. Hayazawa, T. Yano, and S. Kawata, "Highly reproducible tip-enhanced Raman scattering using an oxidized and metallized silicon cantilever tip as a tool for everyone," J. Raman Spectrosc. **43**, 1177–1182 (2012).
[23]L. Novotny, "Allowed and forbidden light in near-field optics. 1. A single dipolar light source," J. Opt. Soc. Am. A **14**, 105–113 (1997).
[24]R. Ossikovski, Q. Nguyen, and G. Picardi, "Simple model for the polarization effects in tip-enhanced Raman spectroscopy," Phys. Rev. B **75**, 045412 (2007).
[25]R. Ossikovski, Q. Nguyen, G. Picardi, and J. Schreiber, "Determining the stress tensor in strained semiconductor structures by using polarized micro-Raman spectroscopy in oblique backscattering configuration," J. Appl. Phys. **103**, 093525 (2008).
[26]A. Jorio, A. G. S. Filho, V. W. Brar, A. K. Swan, M. S. Unlu, B. B. Goldberg, A. Righi, J. H. Hafner, C. M. Lieber, and R. Saito, "Polarized resonant Raman study of isolated single-wall carbon nanotubes: Symmetry selection rules, dipolar and multipolar antenna effects," Phys. Rev. B **65**, 121402 (2002).
[27]H. Yoshida, K. Inaba, and N. Sato, "X-ray diffraction reciprocal space mapping study of the thin film phase of pentacene," Appl. Phys. Lett. **90**, 181930 (2007).
[28]T. Mino, Y. Saito, H. Yoshida, and P. Verma, "Molecular orientation analysis of organic thin-films by Z-polarization Raman-microscope," J. Raman Spectrosc. **43**, 2029–2034 (2012).
[29]C. D. Dimitrakopoulos and P. R. L. Malenfant, "Organic thin film transistors for large area electronics," Adv. Mater. **14**, 99 (2002).
[30]N. Hayazawa, Y. Saito, and S. Kawata, "Detection and characterization of longitudinal field for tip-enhanced Raman spectroscopy," Appl. Phys. Lett. **85**, 6239–6241 (2004).
[31]X. Yan, T. Suzuki, Y. Kitahama, H. Sato, T. Itoh, and Y. Ozaki, "A study on the interaction of single-walled carbon nanotubes (SWCNTs) and polystyrene (PS) at the interface in SWCNT–PS nanocomposites using tip-enhanced Raman spectroscopy," Phys. Chem. Chem. Phys. **15**, 20618–20624 (2013).
[32]X. Wang, H. J. Egelhaaf, H. G. Mark, H. Azimi, C. Brabec, A. J. Meixner, and D. Zhang, "Morphology related photo-degradations of low band-gap polymer blends," Adv. Energy Mater. **4**, 1400497 (2014).
[33]P. C. Sevinc, X. Wang, Y. Wang, D. Zhang, A. J. Meixner, and H. Peter Lu, "Simultaneous spectroscopic and topographic near-field imaging of TiO_2 single surface states and interfacial electronic coupling," Nano Lett. **11**, 1490–1494 (2011).